RSC Advances

ROYAL SOCIETY OF CHEMISTRY

www.rsc.org/advances

RSC Advances

ARTICLE

Influence of the Side-Chain Structure and Molecular Weight on the Re-entrant Behaviors of Mesogen-Jacketed Liquid Crystalline Polymers

Received 00th January 20xx,
Accepted 00th January 20xx

DOI: 10.1039/x0xx00000x

www.rsc.org/

Zheng Xiang, Sheng Chen*, Yongbing Luo, Ping Li, Hailiang Zhang *

Three series of mesogen-jacketed liquid crystalline polymers (MJLCPs) containing different terminal groups (phenmethyl, diphenylmethyl and triphenylmethyl) in the side chains, abbreviated named Pv-m-Bn, Pv-m-DPM, Pv-m-Tr (m =2, 4, 6, 8, 10, 12, which was the number of the methylene units between the terephthalate core and terminal groups in the side chains), were designed and successfully synthesized via free radical polymerization. The molecular characterizations of the polymers were performed with ^{1}H NMR, GPC and TG analysis. The phase structures and transitions of the polymers were investigated by the combination of techniques including DSC, POM and 1D/2D WAXD. The experimental results revealed that all polymers exhibited excellent thermal stabilities and the re-entrant behaviors of MJLCPs were found to be strongly dependent on the structure of the side-chain, that was, the spacer length was increased with the increasing volume of the terminal groups when the polymers wanted to exhibit the re-entrant isotropic phase. On the other hand, a series of MJLCPs, poly {2,5-bis[(diphenylmethoxy-ethyl)oxycarbonyl]-styrenes} (Pv-2-DPMs), with different molecular weights (M_n) and narrow M_n distributions have been successfully synthesized via ATRP. The results indicated that when the M_n were below 1.73 × 10^4 g/mol, only isotropic phase was observed. When M_n was between 3.40 × 10^4 g/mol and 8.48 × 10^4 g/mol, a re-entrant isotropic phase in low temperature and columnar nematic phase in high temperature were formed. Further increasing the M_n to exceed 9.71 × 10^4 g/mol, a stable columnar nematic phase was developed. This work provides two effective ways to design and synthesize MJLCPs with re-entrant behaviors, meantime, it is meaningful to deeply understand the structure–property relationships of MJLCPs.

1. Introduction

In the past decades, liquid crystalline polymers (LCPs) have attracted considerable attention. This is a consequence not only for their scientific interests but also from an industrial point of view due to their potential applications in fields such as engineering plastics, optical data storage, optic, electro-optic, nonlinear optic devices, photomechanical and so on.[1-10] Those applications strongly depend on the phase structures and phase transitions of LCPs. Therefore, many researchers have investigated the structure–property relationship of LCPs in order to understand the principles of structure formation and structure manipulation.

In general, LCPs have two main categories: main-chain liquid crystalline polymers (MCLCPs) with mesogen units located in the main chain[11-13] and side-chain liquid crystalline polymers (SCLCPs) with mesogens attached to the main chain as side groups[14-16], which can be readily obtained by attaching anisotropic mesogens to the backbone via a flexible spacer,[17] with an excellent combination of liquid crystalline (LC) and polymer characteristics. The flexible spacers between the side-chain mesogen and the backbone decouple the motions of mesogens and main chains, facilitating the formation of LC phases. Later, Zhou et al.[18] had reported a special type of side-on SCLCPs called mesogen-jacketed liquid crystalline polymers (MJLCPs), which had a short spacer or with a single covalent bond connecting the mesogen to the polymer backbone. The "jacketing effect" owing to steric hindrance forces the main chain to take an extended-chain conformation, leading to the MJLCPs display many thermotropic properties characterized by MCLCPs, although they belong to SCLCPs chemically, such as high glass transition temperature, broad LC temperature range, and forming banded texture after mechanical shearing in LC state. Based on the concept of the "jacketing effect", many researchers have investigated the structure-property relationship of MJLCPs to understand the principles of structure formation and structure manipulation.[19,20] For example, our group has researched the reentrant isotropic phase behavior of MJLCPs.[21,22]

Re-entrant phase is an exceptional case in LC physics, as they violate the second law of thermodynamics that molecular order should decrease with the increase of temperature,[23] which was first discovered by Yu et al. when they studied the lauric acid potassium solution in 1980. Currently, the re-entrant phase behavior basically can be divided into three categories, namely reentrant isotropic phase, re-entrant nematic phase and re-entrant columnar phase. At

Key Laboratory of Polymeric Materials and Application Technology of Hunan Province, Key Laboratory of Advanced Functional Polymer Materials of Colleges and Universities of Hunan Province, College of Chemistry, Xiangtan University, Xiangtan 411105, Hunan Province, China. E-mail: huaxuechensheng@163.com Electronic Supplementary Information (ESI) available: More detailed synthesis and characterization See DOI: 10.1039/x0xx00000x

present, two main classes of thermotropic LC polymers with re-entrant phase behavior have been studied. One is end-on SCLCPs based on mesogenic units containing a cyano group with five or six atoms in the flexible spacer and a polyacrylate or poly(vinyl ether) backbone.[24-27] These polymers exhibit a reentrant nematic phase due to the frustration induced by competing order parameters that favor different periodicities. The other is dendritic LCPs and MJLCPs, which exhibits a reentrant isotropic phase.[21,22,28-37] For example, Percec et al.[28] have studied poly{4-[3,4,5-tris(n-dodecanyloxy)benzoyloxy]-4-(2-vinyloxyethoxy)biphenyl}, and found that as the DP was about 4 to 5, the polymer exhibited re-entrant isotropic phase. Zhu et al.[32,38] have synthesized a MJLCP containing triphenylene (Tp) moieties in the side chains with 12 methylene units as spacers. The experiment results showed that the low-temperature phase of the polymer was a hexagonal columnar phase self-organized by Tp discotic mesogens. The high-temperature phase was a nematic columnar phase with a larger dimension developed by the rod-like supramolecular mesogen—the MJLCP chain as a whole. A re-entrant isotropic phase was found in the medium temperature range.Yin et al.[33] and Chen et al.[21] have reported the synthesis and characterization of a series of novel MJLCPs with different length alkyl tail named poly[di(alkyl)vinylterephthalates] (P-m) and poly{2,5-bis[(4-alkoxyphenyl)oxycarbonyl]styrenes} (P-OCm) respectively. When m=6, 8, 10, the P-m exhibited the re-entrant isotropic phase, the P-OCm, showed the re-entrant isotropic phase when m>4. Yu et al.[30] and Zhu et al.[31] also found that poly[2,5-bis(4'-alkoxycarbonylphenyl)styrene]s and poly[2,5-bis(4'-alkoxyphenyl)-styrene] both exhibited the re-entrant isotropic phase when the alkyl tail length exceeded a minimum critical length.

Beside the structural factors, the re-entrant behavior of the MJLCPs is also influenced by the M_n. Zhao et al.[29] has reported reentrant phase behavior of MJLCPs based on [poly-{2,5-bis[(4-butoxyphenyl)oxycarbonyl]styrene}] (PBPCS), which were synthesized by ATRP (Atom Transfer Radical Polymerization). The samples with M_n below 2.42×10^4 g/mol were isotropic. The samples with M_n exceed 3.36×10^4 g/mol displayed a thermodynamically stable isotropic phase at lower temperature and a LC phase at higher temperature. Our group has synthesized a series of MJLCPs via ATRP, poly{2,5-bis[(4-octa-decyloxyphenyl)oxycarbonyl]-styrenes} (P-OC18s).[22] The results indicated that the polymers formed a smectic phase at low temperature and an isotropic phase at high temperature when the M_n is lower than a critical M_n of approximately 4.6×10^4 g/mol. The samples with $M_n \geq 5.2 \times 10^4$ g/mol displayed a reentrant isotropic phase.

In this study, in order to deep understand the relationship between the chemical structure and M_n to the reentrant behavior of the MJLCPs, series of MJLCPs have been synthesized via changing the length of spacer and the volume of side group, named poly {2,5-bis[(phenmethyl-alkyl)oxycarbonyl]-styrenes} Pv-m-Bn and poly {2,5-bis[(diphenylmethoxy-alkyl)oxycarbonyl]-styrenes} Pv-m-DPM (m=2, 4, 6, 8, 10, 12, which is the number of the methylene units between the terephthalate core and terminal groups in the side chains). Combined with the results of the poly{2,5-bis[(triphenylmethoxy-alkyl)oxycarbonyl]-styrenes} (Pv-m-Tr),[39] it revealed that all polymers exhibited excellent thermal stabilities and the re-entrant behaviors of MJLCPs were found to be strongly dependent on the side-chain structure and M_n. The spacer length for the re-entrant behaviors of the polymers is increased with the increasing volume of the terminal groups.

Meantime, a series of MJLCPs with different M_ns have been prepared by ATRP polymerization, named poly {2,5-bis[(diphenylmethoxy-ethyl)oxycarbonyl]-styrenes} (Pv-2-DPMs). It was the first time to find that the MJLCPs presented isotropic phase→re-entrant isotropic phase→ columnar phases with the increase of M_n. All the chemical structures of the polymers are shown in Scheme 1.

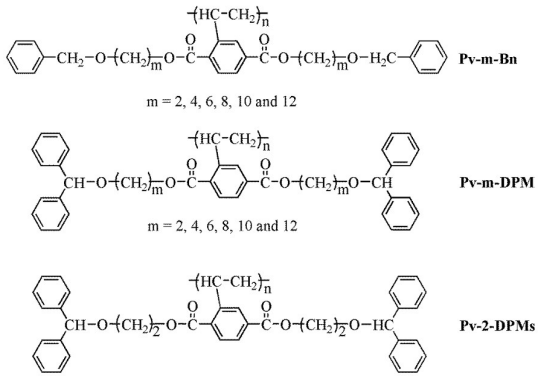

Scheme 1: Chemical structures of the polymers

2. Experimental

2.1. Materials

Anhydrous tetrahydrofuran (THF) was distilled from sodium benzophenone ketyl under argon and used immediately. Triethylamine (TEA) and dichloromethane (CH_2Cl_2) were dried over magnesium sulfate anhydrous. Chlorobenzene (Acros 99 %) was purified by washing with concentrated sulfuric acid to remove residual thiophenes, followed by twice washing, first with 5 % sodium carbonate solution, and then with water before it was dried with anhydrous calcium chloride and distilled. Cuprous bromide (CuBr) was synthesized from $CuBr_2$, purified by stirring in acetic acid, and washing with methanol and then dried in a vacuum just before use. 2, 2-azobisisobutyronitrile (AIBN) was freshly recrystallised from methanol. *N, N, N', N'', N''*-Pentamethyldiethylenetriamine (PMDETA) (99.5 %) and 2-bromoisobutyryl bromide were used as received without further purification. All other reagents and solvents were used as received without further purification.

2.2. Instruments and measurements

^{1}H NMR spectroscopy was performed on a Bruker ARX400 MHz spectrometer using with $CDCl_3$ as solvent, tetramethylsilane (TMS) as the internal standard at ambient temperature. The chemical shifts were reported on the ppm scale.

The apparent number average molecular weight (M_n) and polydispersity index (PDI = M_w/M_n) were measured on a GPC (WATERS 1515) instrument with a set of HT3, HT4 and HT5. The μ-styragel columns used THF as an eluent and the flow rate was 1.0

ml /min at 38 °C. All the GPC data were calibrated with polystyrene

standards.

TGA was performed on a TA SDT 2960 instrument at a heating rate of 20 °C /min in nitrogen atmosphere.

DSC traces of the polymer were obtained using a TA Q10 DSC instrument. The temperature and heat flow were calibrated using standard materials (indium and zinc) at a cooling and heating rates of 10 °C /min. The sample with a typical mass of about 5 mg was encapsulated in sealed aluminum pans.

LC texture of the polymers was examined under POM (Leica DM-LM-P) equipped with a Mettler Toledo hot stage (FP82HT).

One-dimensional wide-angle X-ray diffraction (1D WAXD) experiments were performed on a BRUKER AXS D8 Advance diffractometer with a 40 kV FL tubes as the X-ray source (Cu Kα) and the LYNXEYE_XE detector. Background scattering was recorded and subtracted from the sample patterns. The heating and cooling rates in the 1D WAXD experiments were 10 °C /min.

Two-dimensional wide-angle X-ray diffraction (2D WAXD) was carried out using a BRUKER AXS D8 Discover diffractometer with a 40 kV FL tubes as the X-ray source (Cu Kα) and the VANTEC 500 detector. The point-focused X-ray beam was aligned either perpendicular or parallel to the mechanical shearing direction. For both the 1D and 2D WAXD experiments, the background scattering was recorded and subtracted from the sample patterns.

2.3. Synthesis of monomers

The synthetic route of Mv-m-Bn and Mv-m-DPM are outlined in Scheme 2 and 3[21, 40, 41]. And the detail information about the intermediate and monomers were shown in supporting information.

2.4. Synthesis of polymers

The polymers [Pv-m-Bn and Pv-m-DPM in Scheme 2 and 3] were synthesized by conventional solution radical polymerization. For example, 0.30g (0.41 mmol) of Pv-6-DPM, 40 μL of THF solution of 10 mg/mL AIBN, 0.66 mL of THF and a magnetic stir bar were added into a polymerization tube, the tube was purged with nitrogen and subjected to four freeze-thaw cycles to remove any dissolved oxygen and sealed off under vacuum. Polymerization was carried out at 70 °C for 12 h. The tube was then opened, and the reaction mixture was diluted with 9 mL of THF. Then, the resultant polymer was dropped slowly into the mixture of methanol/THF (4/1). The dissolution and precipitation were repeated three times. After drying under vacuum, 0.21 g of polymer was obtained. Yield: 70%.

In addition, the polymers Pv-2-DPMs with different M_ns were successfully synthesized by ATRP, and detailed synthetic procedures were showed in S2.

3. Results and discussion

3.1. Synthesis and characterization of monomers and corresponding polymers

As shown in Scheme 2 and 3, all the monomers were synthesized by only two steps. The structures of the monomers were confirmed through ^{1}H NMR, IR (see S3) and mass spectrometry measurements.

All the monomers could be easily polymerized via free radical polymerization. Herein, we use Pv-6-DPM as an example to

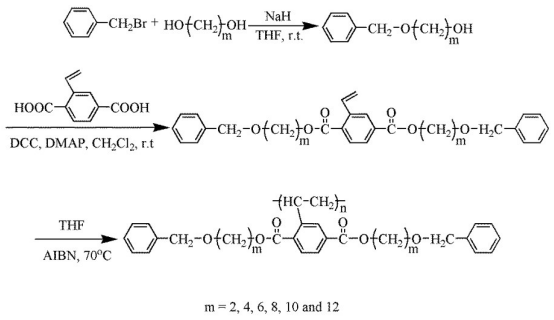

Scheme 2: Synthetic route of the monomers (Mv-m-Bn) and the corresponding polymers (Pv-m-Bn)

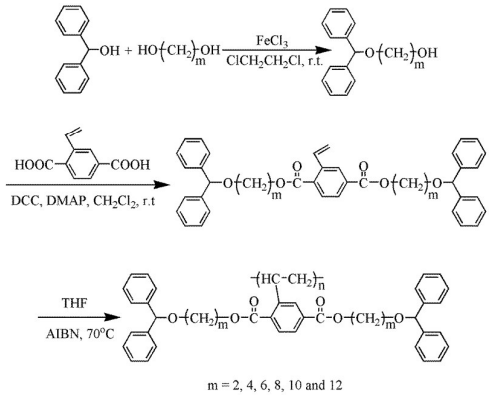

Scheme 3: Synthetic route of the monomers (Mv-m-DPM) and the corresponding polymers (Pv-m-DPM)

elucidate the process. Figure 1(a) and (b) give the ^{1}H NMR spectra ($CDCl_3$[-d]) of the monomer Mv-6-DPM and the polymer Pv-6-DPM, respectively. Mv-6-DPM showed characteristic resonances of the vinyl group at 5.39-5.76 ppm. After polymerization, the signals disappeared completely. The adsorption peaks of Pv-6-DPM were quite broad and consistent with the expected polymer structure. In addition, the IR spectra of Mv-6-DPM and Pv-6-DPM was showed in Figure S2. Obviously, the out-of-plane vibration of vinyl group disappeared after polymerization. The apparent number-average molecular weights of the polymers determined by GPC were higher than 1×10^5 g/mol, demonstrating good polymerizability of the monomers. The molecular characterizations of the polymers were summarized in Table 1 and Table 2, respectively.

The polymers (Pv-2-DPMs) with different M_n were successfully synthesized by ATRP. The GPC curves were shown in Figure S3 and the results were summarized in Table S1. The M_n was gradually increased from 1.73×10^4 to 13.65×10^4 g/mol. Furthermore, the polydispersity of the polymers was even lower than the theoretical value of 1.30 for the controlled "living" free radical polymerization.

3.2. Thermal and liquid-crystalline properties of the polymers

The thermal and liquid-crystalline properties of the polymers (Pv-m-Bn, Pv-m-DPM and Pv-2-DPMs) were investigated by DSC and POM. Before, the polymers (Pv-m-Bn and Pv-m-DPM) were investigated by TGA. As shown in Table 1 and 2, all polymers exhibited excellent thermal stabilities with the temperatures at 5% weight loss about 350 °C in nitrogen.

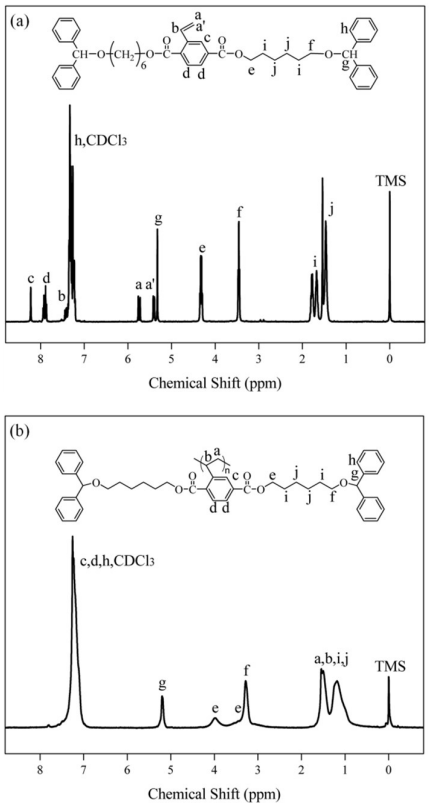

Figure 1: ^{1}H NMR spectrums of the monomer Mv-6-DPM (a) and the polymer Pv-6-DPM (b) in $CDCl_3$

The phase-transition behaviors of the polymers were investigated by DSC. The samples firstly were heated from ambient temperature to 300 ^{o}C at a rate of 20 ^{o}C /min under nitrogen atmosphere to eliminate the thermal history. Figure 2, Figure 3 and Figure S5 showed the DSC curves of Pv-m-Bn, Pv-m-DPM and Pv-2-DPMs at a rate of 10 ^{o}C /min respectively.

For the series of Pv-m-Bn (m =2, 4, 6, 8, 10, 12), Figure 2(a) and (b) showed the second heating and the first cooling DSC curves of Pv-m-Bn at a rate of 10 ^{o}C /min respectively. The polymer Pv-2-Bn showed a clear glass transition (T_g') temperature during the first cooling at -8.0 ^{o}C, however, no peaks was detected when the second heating. For the polymers Pv-4-Bn and Pv-6-Bn, they showed T_g whatever heating or cooling. For Pv-8-Bn, we could not find any peak, but the polymers Pv-10-Bn and Pv-12-Bn showed a significant transition peak during the heating and cooling processes at -46.4 ^{o}C and -31.9 ^{o}C, possibly as a result of the melting and crystallization of the alkyl chain. The results are shown in the Table 1.

For the series of Pv-m-DPM (m=2, 4, 6, 8, 10, 12), Figure 3(a) and (b) showed the second heating and the first cooling DSC curves of Pv-m-DPM at a rate of 10 ^{o}C /min respectively. All samples exhibited a single and obvious T_g when heating or cooling. As expected, T_g decreases from 45.2 ^{o}C to -33.0 ^{o}C as the spacer length increases owing to the strong internal plasticization effect of the longer alkyl spacers and the results are listed in Table 2. No other transition peak was observed except T_g and this phenomenon was found in the other MJLCPs.

Figure S5(a) and (b) showed the second heating and the first cooling DSC curves of Pv-2-DPM with different M_ns at a rate of 10 ^{o}C /min respectively. A single and obvious T_g was observed under heating-cooling cycles, and the T_g increased slightly from 44.4 ^{o}C to 45.8 ^{o}C with the increase of the M_n. This implied when the M_n of polymer exceed 1.73×10^4 g/mol, the M_n of polymer has no effect on the T_g of the polymer.

Polarized optical microscopy (POM) was used to investigate the liquid crystallinity of the polymers. To be consistent with the DSC result (the second heating), the testing condition was the same as DSC. For the series of Pv-m-Bn, the results showed that the polymers can be divided into two types. The first one was the Pv-m-Bn (m=2, 10 and 12). No birefringence was detected by POM, implying the absence of the thermotropic mesophase. The second one was the Pv-m-Bn (m=4, 6 and 8). On heating process, the sample became soft above the T_g, but there was no birefringence to be seen, indicating the formation of isotropic phase. Then, the granular LC texture was observed when the temperature reached about 160, 139, and 237 ^{o}C, respectively. Figure 4 showed the POM images of the representational sample Pv-6-Bn at low temperature [Figure 4(a)] and high temperature [Figure 4(b)]. With furthering heating, no visible change of birefringence was observed before decomposition (onset temperature > 300 ^{o}C). On the subsequent cooling, the original scene was reestablished, that was, the birefringence disappeared. Therefore, based on our previous research,[21] the former polymers were amorphous polymers, but the latter were the first kind of MJLCPs with a re-entrant phase.[29, 31]

In order to observe the phase transition temperature intuitively, we performed reflection light intensity (birefringence) measurements. While the phase transition process from isotropic phase to LC phase, it could not be detected by DSC but reflection light intensity measurements, because the thermal enthalpy change was extremely small. Figure 5 showed the recorded changes in reflection light intensity for Pv-4-Bn, Pv-6-Bn and Pv-8-Bn by POM at a rate of 10 ^{o}C /min. As can been seen, an obvious transition peak appeared at 160 ^{o}C, 139 ^{o}C and 237 ^{o}C (T_1) respectively, in which the reflection light intensity sharply increased to 56% from 11%, showing a transition from isotropic state to ordered state.[42] When cooling, the change of intensity was slower than heating process, indicating after the polymer formed columnar phase, the polymer could keep the order structure in some degree to reduce the influence of driving force of the entropy (see Figure S4) .

For the series of Pv-m-DPM, the results showed that the polymers can be divided into three types. The first one was the Pv-m-DPM (m=2, 4 and 6). They exhibited strong birefringence that remained invariably even when heated to 300 ^{o}C or subsequently cooled to room temperature. All these polymers showed the stable needle texture and the POM image of polymer Pv-6-DPM was shown in Figure 6(a), suggesting the formation of columnar phase. Second one was Pv-8-DPM in which phase transition was the same as the Pv-m-Bn (m=4, 6 and 8), and the transition temperature from isotropic phase to the LC phase was about 126 ^{o}C. Figure 6(b) and Figure 6(c) showed the POM image of polymer at isotropic phase and LC phase respectively. The last one was the Pv-m-DPM (m=10

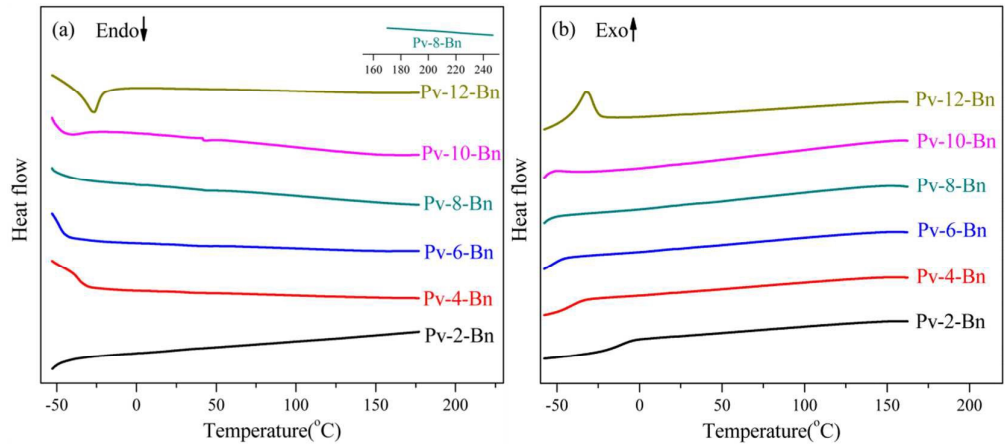

Figure 2: DSC curves of polymers Pv-m-Bn during the second heating scan (a) and the first cooling scan (b) at a rate of 10 °C /min under nitrogen atmosphere

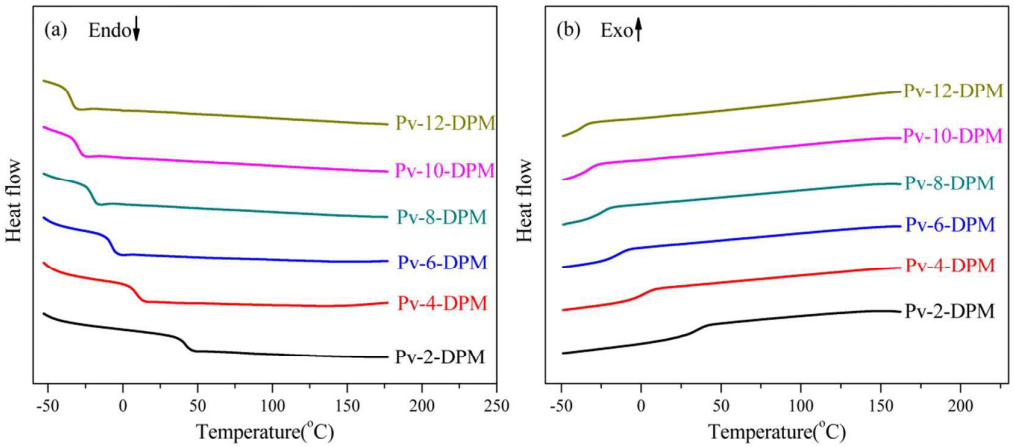

Figure 3: DSC curves of polymers Pv-m-DPM during the second heating scan (a) and the first cooling scan (b) at a rate of 10 °C /min under nitrogen atmosphere

and 12). No birefringence was detected by POM, indicating the absence of the thermotropic mesophase. In general, Pv-m-DPMs can be classified into three types. The first type of the polymers (m=2, 4 and 6) were transitional MJLCPs, while the second one (m=8) was the first kind of MJLCPs with a re-entrant phase,[29, 31] and the last one (m=10 and 12) was amorphous polymer.

Figure 7 shows the recorded changes in reflection light intensity for Pv-6-DPM and Pv-8-DPM by POM at a rate of 10 °C /min. From the curves, there was little change for the intensity of Pv-6-DPM and the reflection light intensity kept at 59%. However, for Pv-8-DPM, an obvious transition peak appeared at 126 °C (T_1) in which the reflection light intensity sharply increased to 55% from 11%, showing a transition from isotropic state to ordered state.[42] When cooling, the reflection light intensity returned to the original state (see Figure S4).

For the series of Pv-2-DPMs, the POM results showed that the polymers can also be divided into three types. The first one was P1. No birefringence was detected by POM. The second kind was P2-P5. The observation results were similar with the Pv-m-Bn (m=4, 6 and 8) and Pv-8-DPM. Taking P3 as the example, the POM pictures were shown in Figure 8(a) and Figure 8(b). And the transition temperature from isotropic phase to the LC phase was about 162 °C. The third type was P6-P7. The samples exhibited the stable texture and the LC birefringence unchanged even when heated to 300 °C. While cooling to room temperature from 300 °C, the birefringence of the sample remained unchanged, showing that the ordered structure kept unchanged upon cooling. So the polymers were amorphous when M_n below 1.73 × 10^4 g/mol. The polymers belonged to the first kind of MJLCPs with a re-entrant phase when M_n between 3.40 × 10^4 g/mol and 8.48 × 10^4 g/mol.[29, 31] Lastly, the polymers were transitional MJLCPs when M_n exceeds 9.71 × 10^4 g/mol.

Figure 9 shows the recorded changes in reflection light intensity for P1-P6 by POM at a rate of 10 °C /min. For the P1 and P6, there was little change for the intensity and the reflection light intensity kept at 7% and 72%, respectively. However, P2-P5 showed obvious transition peak appeared at 224 °C, 162 °C, 143 °C and 137 °C (T_1) in which the reflection light intensity sharply increased to 64% from 7%, showing a transition from isotropic state to ordered state,[42] and the transition temperature was decreased with the increasing of M_n.

3.3. Phase structure identification of the polymers

To further characterize the mesomorphic structure of Pv-m-Bn, Pv-m-DPM and Pv-2-DPMs, temperature-dependent powder 1D WAXD was used. About 60 mg of the polymer was added into an aluminum foil substrate. The testing conditions were consistent with the DSC and POM measurements.

Table 1: Molecular characteristics and properties of the series of Pv-m-Bn

Sample	M_n (×10^{-5})[a]	PDI[a]	T_d (°C)[b]	T_m (°C)[c]	T_g (°C)[c]	T_g' (°C)[c]	T_1 (°C)[d]	Liquid crystallinity[d]
Pv-2-Bn	1.85	1.87	365			-8.0		No
Pv-4-Bn	1.05	1.83	350		-32.4	-36.5	160	Yes
Pv-6-Bn	1.14	1.91	359		-44.0	-46.4	139	Yes
Pv-8-Bn	1.53	1.83	369				237	Yes
Pv-10-Bn	1.24	1.81	344	-46.4				No
Pv-12-Bn	1.01	1.80	358	-31.9				No

Table 2: Molecular characteristics and properties of the series of Pv-m-DPM

Sample	M_n (×10^{-5})[a]	PDI[a]	T_d (°C)[b]	T_g (°C)[c]	T_1(°C)[d]	Liquid crystallinity[d]
Pv-2-DPM	1.32	1.95	361	45.2		Yes
Pv-4-DPM	1.21	2.16	355	10.8		Yes
Pv-6-DPM	1.93	2.01	349	-5.0		Yes
Pv-8-DPM	1.27	1.81	358	-19.2	126	Yes
Pv-10-DPM	1.42	1.75	358	-27.5		No
Pv-12-DPM	1.13	1.85	346	-33.0		No

[a] The apparent number-average molecular weight (Mn) and polydispersityindex (PDI) were measured by GPC using PS standards.

[b] The temperatures of 5% weight loss under nitrogen were measured by TGA heating experiments at a rate of 20 oC /min.

[c] The melting temperatures (Tm) and the glass transition temperatures (Tg) during the second heating process and the glass transition temperatures (Tg') during the first cooling process were all measured by DSC at a rate of 10 °C /min under a nitrogen atmosphere.

[d] Evaluated by POM at a heating and cooling rate of 10 °C /min.

For the series of Pv-m-Bn and Pv-m-DPM, 1D WAXD experiment results were consistent with the POM results. Figure 10(a) and 10(b) illustrated the temperature variable 1D WAXD patterns of Pv-6-DPM during the second heating (30-250°C) and subsequent cooling (250-30°C). And the test region of 2θ was from 1.5° to 35°. In the low angle region, one narrow reflection peak was observed at 2θ = 4.22° (d = 2.09 nm), demonstrating that the ordered structures at the nanometer scale formed. The intensity of the halo basically kept the same with the temperature elevated, i.e., 250 °C. When cooling down, the diffraction peak intensity unchanged, suggesting that polymer always kept the ordered structures in the whole temperature. In the high angle region, only an amorphous halo around 20° could be recognized. This reflected that no long range ordered structure formed via molecular packing was detected over the entire temperature region studied. In addition, no noticeable change could be observed during the second heating and cooling processes in 1D WAXD experiments, implying that there was no isotropic phase for Pv-6-DPM in the temperature region from 30 to 250 °C. 1D WAXD patterns of Pv-2-DPM and Pv-4-DPM were similar to those of Pv-6-DPM. Therefore, Pv-m-DPM (m=2, 4 and 6) probably forms a stable columnar phase.

Figure 11(a) and 11(b) showed the structurally sensitive 1D WAXD patterns of Pv-8-DPM. When the temperature was below 100 °C, the low-angle diffraction peak was diffuse and weak. When temperatures were above 100 °C, a sharp and intense peak at 2θ = 3.81° (d = 2.32 nm) appeared. With the further increasing temperature, the intensity of the peak increases. The peak became weak and disappeared at 100 °C on the following cooling scan [see Figure 11 (b)]. The distinct discontinuous intensities corresponded with the endothermal transition of POM at about 130 °C during the second heating. The discontinuous observation during cooling procedure clearly indicated that the LC phase formed at higher temperature disappeared during cooling. Those implied that the Pv-8-DPM formed the re-entrant phase and similar results were obtained from Pv-m-Bn (m =4, 6, 8).

However, for the Pv-m-Bn (m=2, 10, 12) and Pv-m-DPM (m = 10, 12), no low angle scattering peaks were observed in the 1D WAXD patterns during the heating and cooling processes, suggesting that they were amorphous throughout the temperature region.

Figure 12 (a) and 12(b) depict two sets of 1D WAXD patterns for Pv-m-Bn and Pv-m-DPM (m = 2, 4, 6, 8, 10, 12) samples obtained at 250 °C, and the data of all polymers at 250 °C are summarized in Table 3 and Table 4. The results showed that the d-spacing value increases with the increase of m.

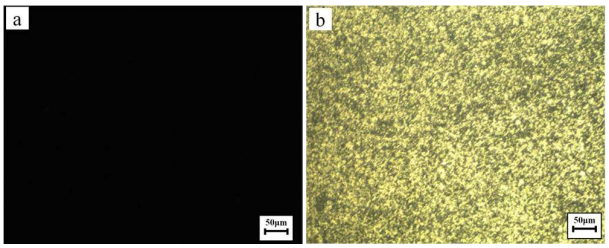

Figure 4: Representative POM images of the texture of the Pv-6-Bn maintained at 100 °C(a) and 180 °C(b) (Magnification: ×200).

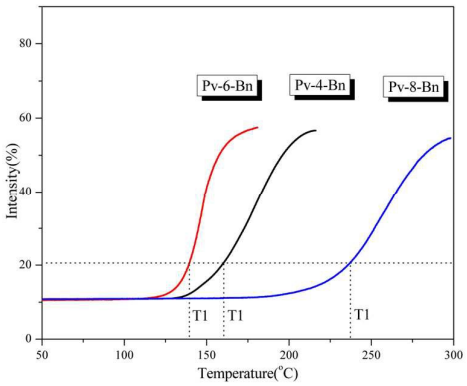

Figure 5: The change of reflection light intensity for Pv-4-Bn, Pv-6-Bn and Pv-8-Bn at a heating rate 10 °C/min in POM

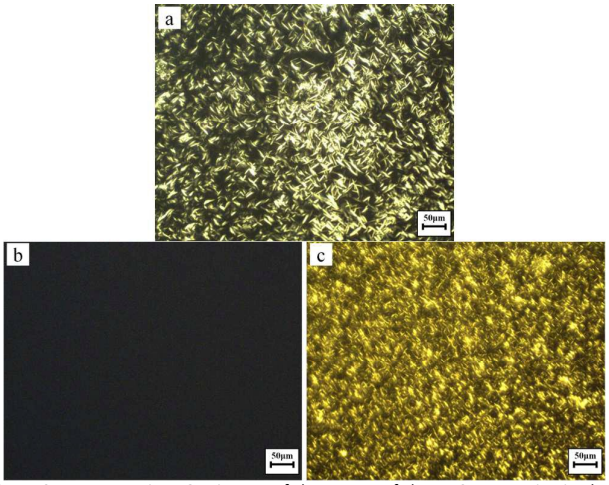

Figure 6: Representative POM images of the texture of the Pv-6-DPM maintained at 180 °C(a), and representative POM images of the texture of the Pv-8-DPM maintained at 100 °C(b) and 180 °C(c) (Magnification: ×200).

1D WAXD experiment results for the Pv-2-DPMs showed that the samples could also be divided into three types. The first type was P1, no low angle scattering peaks were seen in the 1D WAXD patterns during the heating and cooling processes [as shown in Figure S6(a) and S6(b)]. The second one was P2-P5, taking the P4 as the example, the observation of 1D WAXD was shown in Figure 13. From Figure 13(a), below 130 °C, the low-angle diffraction peak was diffuse and weak. When temperatures were above 130 °C, a sharp and intense peak at $2\theta = 4.42^{o}$ (d = 2.00 nm) appears. This peak becomes weak and disappears at 100 °C on the following cooling scan [see Figure 13(b)], which was similar to Pv-8-DPM [see Figure 11], indicated that the LC phase formed at higher temperature disappeared during cooling. Those suggested that the P4 formed the re-entrant phase, and the polymers (P2, P3, and P5) showed the similar results. The transition temperatures detected by 1D WAXD was decreased with the increasing of M_n, which were consistent with the POM results.

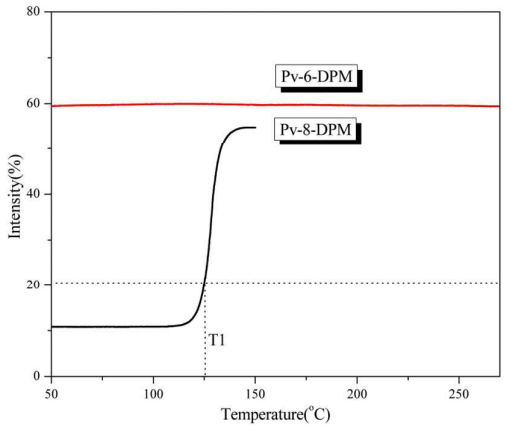

Figure 7: The change of reflection light intensity for Pv-6-DPM and Pv-8-DPM at a heating rate 10 °C/min in POM

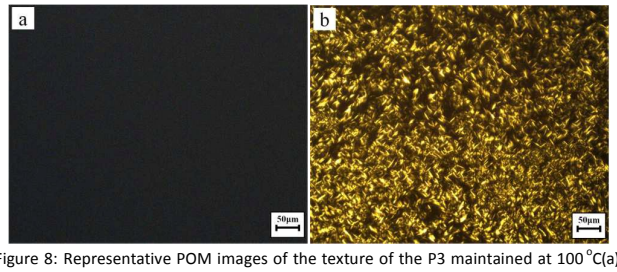

Figure 8: Representative POM images of the texture of the P3 maintained at 100 °C(a) and 180 °C(b) (Magnification: ×200).

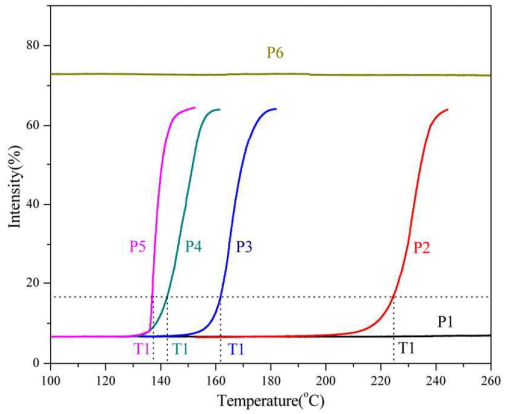

Figure 9: The change of reflection light intensity for P1-P6 at a heating rate 10 °C/min in POM

The third one was P6-P7, taking the P6 as the example, Figure 14 (a) and 14(b) showed the structurally sensitive 1D WAXD patterns of P6 from 30 to 180 °C and from 180 to 30 °C during the second heating and subsequent cooling. The result was similar to the Pv-6-DPM [see Figure 10], just one narrow diffraction peak was observed at the low angle and an amorphous halo at the high angle throughout the heating and cooling processes, illuminated that P6 presented a stable columnar phase. The 1D WAXD patterns for P1-P7 obtained at 250 °C were showed in Figure 15. As can been, the

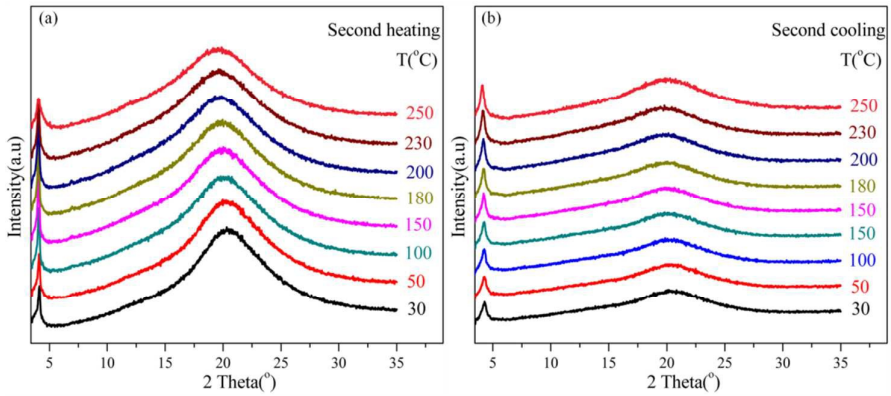

Figure 10: 1D WAXD patterns of Pv-6-DPM during the second heating (a) and subsequent cooling (b)

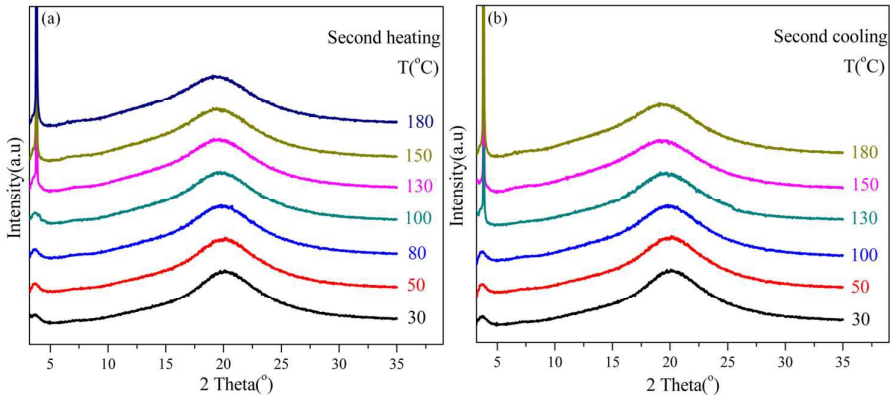

Figure 11: 1D WAXD patterns of Pv-8-DPM during the second heating (a) and subsequent cooling (b)

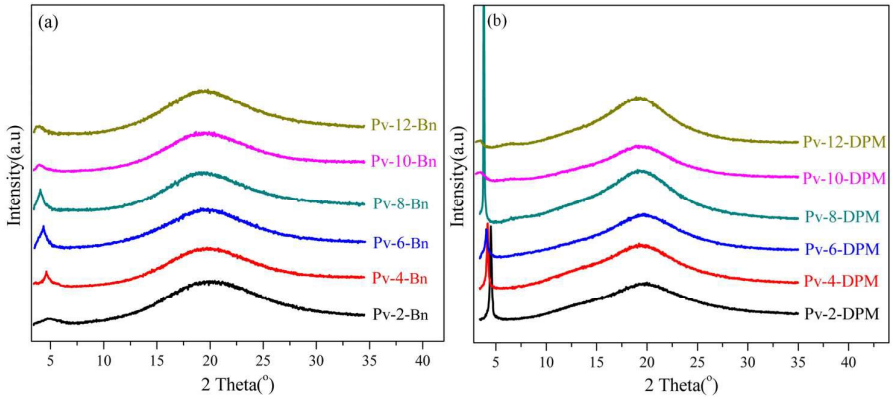

Figure 12: 1D WAXD patterns of Pv-m-Bn (a) and Pv-m-DPM (b) (m = 2, 4, 6, 8, 10 and 12) at 250 °C

2θ value of the narrow reflection peak for P2-P7 at the low angle kept the same, implied that rod diameter of Pv-2-DPMs was not changed with the increasing of the M_n.

2D WAXD was used to further identify the phase structures. All fiber samples were drawn with a pair of tweezers at above glass-transition temperature. Figure 16 showed the 2D WAXD patterns of the polymer Pv-6-DPM at room temperature with X-ray incident beam perpendicular and parallel to the fiber direction. In the Figure 16(a), the fiber axis was perpendicular to the meridian direction. A pair of strong diffraction arcs could be seen on the equator at 2θ = 4.22° (d = 2.09 nm), which was consistent with the 1D WAXD results, indicating that the ordered structures had developed along the direction perpendicular to the fiber axis on the nanometer scale. When the X-ray incident beam was parallel to the shear direction, a ring pattern at 2θ = 4.30° (d = 2.05 nm) was detected, which exhibited an isotropic intensity distribution [Figure 16(b)]. Meanwhile, a diffusion scattering halos in the high 2θ angle were observed, suggesting only the short-range order exists along the fiber direction. Considering the similar X-ray results reported previously,[20,43] we proposed the polymer Pv-6-DPM exhibited a columnar nematic phase. The polymers Pv-m-DPM (m=2 and 4) and P6-P7 showed similar 2D WAXD experiment results, which were

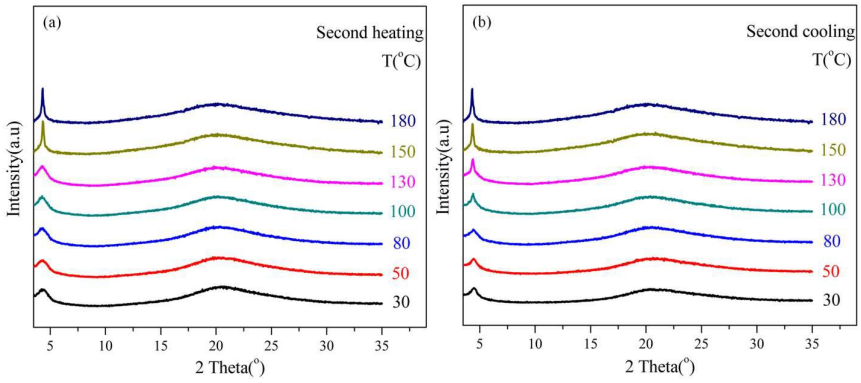

Figure 13: 1D WAXD patterns of P4 during the second heating (a) and subsequent cooling (b)

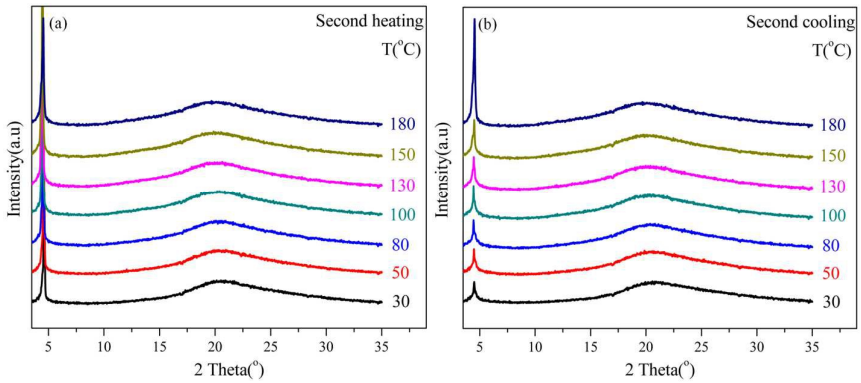

Figure 14: 1D patterns of P6 during the second heating (a) and subsequent cooling (b).

considered to form columnar nematic phase as well as each cylinder is attributed to a single polymer chain with the side groups tightly jacketing the backbone.

For the polymers Pv-m-Bn (m=4, 6, 8), Pv-8-DPM and P2-P5, we could obtain 2D WAXD patterns through the sample heated to 250 °C, then quickly put into the liquid nitrogen to keep the LC phase structure. The 2D WAXD patterns of Pv-6-Bn and Pv-8-DPM were shown in Figure 17. From the patterns, a ring pattern at low 2θ angle and a diffusion scattering halos in the high 2θ angle were presented when the X-ray incident beam was perpendicular to the fiber direction, however, they couldn't be orientated because of the extremely low T_g of these polymers. Combined with the results of POM and 1D WAXD, it was considered for these polymers to form columnar nematic phase at high temperature.

3.4. Influence of the side-chain structure on the phase behaviors

Based on the results of DSC, POM, 1D WAXD and 2D WAXD experiments, the phase behaviors of Pv-m-Bn, Pv-m-DPM and Pv-m-Tr (m=2, 4, 6, 8, 10, 12) were summarized in Figure 18. For the series 1 (Pv-m-Bn) and series 2 (Pv-m-DPM), the polymers show isotropic phase when m is 10 or 12. However, the Pv-10-Tr exhibits a stable columnar nematic phase and the Pv-12-Tr forms a re-entrant phase. On the other hand, the Pv-2-Bn cannot form the LC phase while the Pv-2-DPM and Pv-2-Tr both can present the stable LC phase. Those results can be explained by the steric effect of the side group. The strength of steric effect is determined by the "static steric effect" and "dynamic steric effect". For the strength of "static

Table 3: The2θ d-spacing values and calculated length of the side-chain of Pv-m-Bn

Sample	2θ (°)[a]	d-spacing (nm)[a]	Calculated length of the side-chain (nm)[b]
Pv-2-Bn	—	—	2.58
Pv-4-Bn	4.65	1.90	3.08
Pv-6-Bn	4.34	2.04	3.59
Pv-8-Bn	4.05	2.18	4.12
Pv-10-Bn	—	—	4.54
Pv-12-Bn	—	—	5.16

Table 4: The2θ d-spacing values and calculated length of the side-chain of Pv-m-DPM

Sample	2θ (°)[a]	d-spacing (nm)[a]	Calculated length of the side-chain (nm)[b]
Pv-2-DPM	4.51	1.96	2.59
Pv-4-DPM	4.20	2.10	3.10
Pv-6-DPM	4.02	2.20	3.60
Pv-8-DPM	3.81	2.32	4.10
Pv-10-DPM	—	—	4.52
Pv-12-DPM	—	—	5.14

[a] Obtained from the one-dimensional WAXD experiments.
[b] assuming the n-alkyl spacer in the side chains have an all-trans conformation.

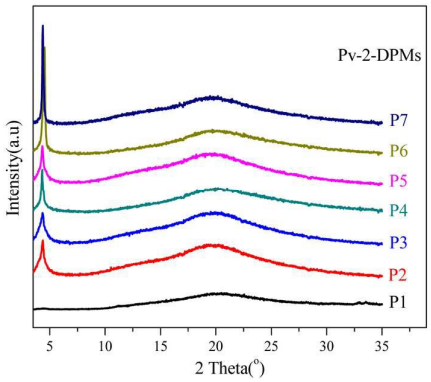

Figure 15: 1D WAXD patterns of P1-P7 at 250 °C

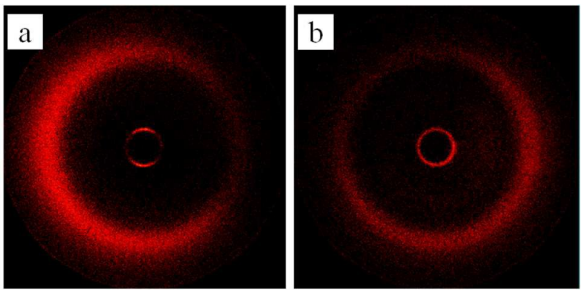

Figure 16: 2D WAXD fiber patterns of Pv-6-DPM. The X-ray incident beam was perpendicular (a) and parallel (b) to the fiber axis.

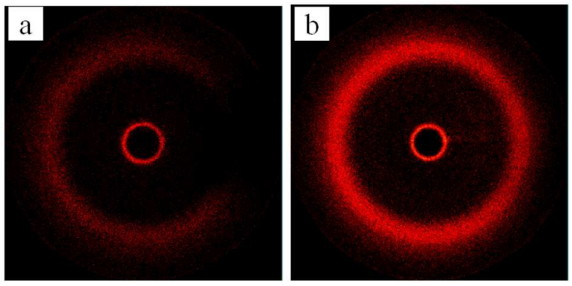

Figure 17: 2D WAXD patterns of Pv-6-Bn (a) and Pv-8-DPM (b) with the X-ray incident beam perpendicular to the fiber direction.

steric effect", it relies on the side-chain structure occupation volume at low temperature, which is related to the rigid, size and shape of side chain. Yet, for the strength of "dynamic steric effect", it relies on the dynamic volumetric of side-chain at high temperature, which is determined by the chemical structure of side-chain and the temperature. As for the Pv-m-Bn, Pv-m-DPM and Pv-m-Tr, the change of terminal group structure from phenmethyl to triphenylmethyl means that the static space volume of side-chain increases. Therefore, it is easy to understand that the Pv-2-Bn cannot display the LC phase due to the weak static steric effect. On the other hand, with increasing benzene ring of terminal group, the critical value of flexible spacer length (m) increases from 4 to 12 when the polymer displays the re-entrant phase (Pv-m-Bn, Pv-m-DPM and Pv-m-Tr). It is caused by the dynamic steric effect. When the spacer (m) increases, the static steric effect becomes weak, leading to that the polymer forms isotropic phase in the low temperature. However, the dynamic steric effect becomes strong in the high temperature, resulting in the formation of LC phase. Furtherly increasing the spacer length, the dynamic steric effect also becomes weak.

Previously, our group has researched the influence of alkyl tail length on the phase behavior and phase structure of poly{2,5-bis[(4-alkoxyphenyl)oxycarbonyl]styrenes} (P-OCm, m=1, 2, 4, 6, 8, 10, 12, 14, 16 and 18). It found that the polymers could show the re-entrant isotropic phase when tail length exceeded a critical value. According to the results of this article, thus, the alkyl spacer length and alkyl tail length play a very important role in the formation of re-entrant phase for the MJLCPs.

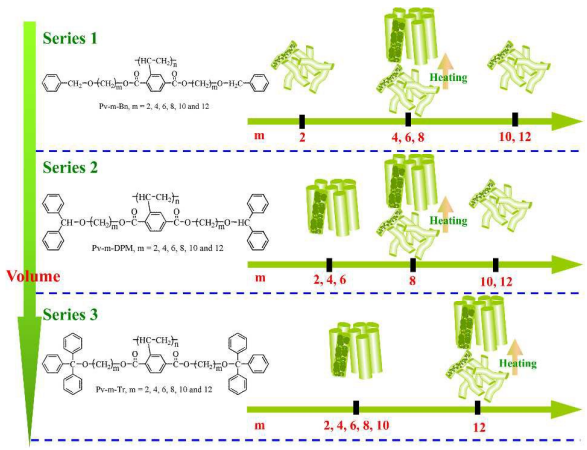

Figure 18: Schematic drawing of the thermotropic phase behavior of the Pv-m-Bn, Pv-m-DPM and Pv-m-Tr (m=2, 4, 6, 8, 10, 12)

3.5. Influence of the molecular weight on the phase behaviors

The evolution of the phase behaviors with increasing the M_n in this series of Pv-2-DPMs can be seen in Figure 19. The phase transitions of the Pv-2-DPMs with middle M_n follow the sequence of reentrant isotropic phase ↔ columnar nematic phase ↔ isotropic phase (it is not true). In the past, Zhao et al.[29] synthesized a series of PBPCS with different M_ns by ATRP and found that phase behavior depended on the M_n. When M_n below 2.42 × 10^4 g/mol, the polymers presented isotropic phase, with the increasing of M_n, the polymer exhibited re-entrant isotropic phase in low temperature and hexagonal columnar phase in high temperature. However, the PBPCS didn't display a stable columnar phase even the M_n was 35.6 × 10^4 g/mol, the Pv-2-DPMs showed a stable columnar phase when

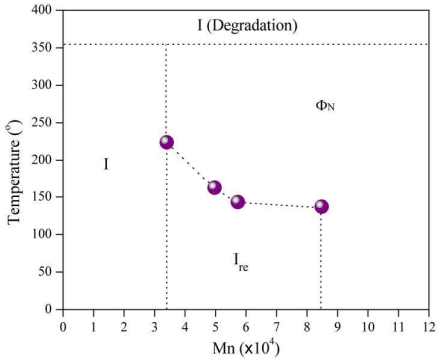

Figure 19: The relationship between the transition temperature and the Mn of Pv-2-DPMs. (I: isotropic phase, Φ_N: columnar nematic phase).

the M_n exceed to 9.71×10^4 g/mol. Therefore, the entropy effect of the side-chain depends strongly on the M_n. The transition temperature of the isotropic phase to the LC phase decreases with the further increasing of the M_n and is even lower than the room temperature.

4. Conclusions

In summary, we have successfully synthesized two series of MJLCPs (Pv-m-Bn and Pv-m-DPM, m=2, 4, 6, 8, 10, 12) with different spacer lengths and terminal groups by free radical polymerization, and a series of MJLCPs (Pv-2-DPMs) with different M_ns by ATRP. The phase structures and transitions of these polymers were investigated by the combined technologies of DSC, POM, and 1D/2D WAXD.

For the series of Pv-m-Bn and Pv-m-DPM, the T_g was decreased with the increasing of m due to the alkyl plastification. The polymers Pv-m-Bn (m=2, 10 and 12) and Pv-m-DPM (m=10 and 12) presented the isotropic phase because of the poor jacketing effect.[44] Pv-m-DPM (m=2, 4 and 6) showed stable columnar nematic phase because of the strong static steric effect. Pv-m-Bn (m=4, 6, 8) and Pv-8-DPM showed the isotropic phase in low temperature and columnar nematic phase in high temperature, because the backbone adopts a somewhat extended conformation due to the consecutive tempestuously motions of side-chain around the main-chain,[45] leading to produce the strong dynamic steric effect with the temperature increased. Combined with the results of the Pv-m-Tr (m=2, 4, 6, 8, 10 and 12), we understand that if the polymers wants to form the re-entrant phase, it needs the longer flexible spacer when the polymers have larger terminal groups.

For the series of Pv-2-DPMs, when M_n below 1.73×10^4 g/mol, only the amorphous state was observed. When M_n between 3.40×10^4 g/mol and 8.48×10^4 g/mol, a re-entrant isotropic phase in low temperature and columnar nematic phase in high temperature formed. Further increasing the M_n to exceed 9.71×10^4 g/mol, a stable columnar nematic phase was developed.

In all, this work provided two facile ways to discover and synthesize the polymers with re-entrant behaviors.

Acknowledgements

This research was financially supported by the National Natural Science Foundation of China (21504075) and the Research Foundation of Education College of Hunan Province, China (Grant No. 14C1090).

Notes and references

1 Z. Q. Yu, T. T. Li, Z. Zhang, J. H. Liu, W. Z. Yuan, J. W. Y. Lam, S. Yang, E. Q. Chen and B. Z. Tang, *Macromolecules*, 2015, **48**, 2886-2893.
2 J. F. Ban, L. N. Mu, L. Chen, S. J Chen and H. L. Zhang, *RSC Adv.*, 2016, **6**, 38790-38796.
3 M. Tian, H. H. Sun, X. W. Tian, Z. X. Xu, F. Q. Wang, D. S. Yao and J. S. Hu, *Liq. Cryst.*, 2015, **42**, 298-308.
4 M. Wang, J. Wang, Hong Yang, B. P. Lin, E. Q. Chen, P. Keller, X. Q. Zhang and Y. Sun, *Chem. Commun.*, 2016, **52**, 4313-4316.
5 S. F. Zhang, C. X. Zhang, J. C. Wang, F. Hong, X. T. Hao, A. Zhang, Y. F. Wang, H. Wu, W. Y. Zhang and J. L. Pu, *Polym. Chem.*, 2016, **7**, 3013-3025.
6 S. Hassan, R. Anandakathir, M. J. Sobkowicz and B. M. Budhlall, *Polym. Chem.*, 2016, **7**, 1452-1460.
7 Z. Y. Zhang, Q. K. Zhang, Z. H. Shen, J. P. Yu, Y. X. Wu and X. H. Fan, *Macromolecules*, 2016, **49**, 475–482.
8 S. Q. Yang, W. Qu, H. B. Pan, Y. D. Zhang, S. J. Zheng, X. H. Fan and Z. H. Shen, *Polymer*, 2016, **84**, 355-364.
9 S. Bronnikov, S. Kostromin, V. Musteaţa and V. Cozan, *J. Polym. Res.*, 2016, **23**, 1-8.
10 H. N. Gayathri, B. Kumar, K. A. Suresh, H. K. Bisoyi and S. Kumar, *Phys. Chem. Chem. Phys.*, 2016, **18**, 12101-12107.
11 M. Tokita, S. Okuda, S. Yoshihara, C. Takahashi, S. Kang, K. Sakajiri and J. Watanabe, *Polymer*, 2012, **53**, 5596-5599.
12 T. S. Jo, A. K. Nedeltchev, B. Biswas, H. Han and P. K. Bhowmik, *Polymer*, 2012, **53**, 1063-1071.
13 C. Ruan, L. Chen, R. Yang, H. Y. Zhong and Y. Z. Wang, *RSC Adv.*, 2015, **5**, 48541-48550.
14 B. Geng, L. X. Guo, B. P. Lin, P. Keller, X. Q. Zhang, Y. Sun and H. Yang, *Polym. Chem.*, 2015, **6**, 5281-5287.
15 Y. S. Xu, D. Shi, J. Gu, Z. Lei, H. L. Xie, T. P. Zhao, S. Yang and E. Q. Chen, *Polym. Chem.*, 2016, **7**, 462-473.
16 X. Q. Liu, J. Wang, S. Yang and E. Q. Chen, *ACS Macro Lett.*, 2014, **3**, 834-838.
17 H. Finkelmann, H. Ringsdorf and J. H. Wendorff, *Makromol. Chem.*, 1978, **179**, 273.
18 Q. F. Zhou, H. M. Li and X. D. Feng, *Macromolecules*, 1987, **20**, 233-234.
19 Y. Y. Qiao, J. Ping, H. J. Tian, Q. K. Zhang, S. Zhou, Z. H. Shen, S. J. Zheng and X. H. Fan, *J. Polym. Sci. Part A: Polym. Chem.*, 2015, **53**, 2116-2123.
20 L. Y. Zhang, H. L Wu, Z. H. Shen, X. H. Fan and Q. F. Zhou, *J. Polym. Sci. Part A: Polym. Chem.*, 2011, **49**, 3207-3217.
21 S.Chen, C. K. Jie, H. L. Xie and H. L. Zhang, *J. Polym. Sci. Part A: Polym. Chem.*, 2012, **50**, 3923-3935.
22 S. Chen, H. Luo, H. L. Xie and H. L. Zhang, *J. Polym. Sci. Part A: Polym. Chem.*, 2013, **51**, 924-935.
23 P. E. Cladis, *Mol. Cryst. Liq. Cryst.*, 1988, **165**, 85-121.
24 W. Renz, *Mol. Cryst. Liq. Cryst.*, 1988, **155**, 549-558.
25 B. I. Ostrovskii, S. N. Sulyanov, N. I. Boiko, V. P. Shibaev and W. H. D. Jeu, *Eur. Phys. J. E.*, 2001, **6**, 277-285.
26 J. C. Dubois, G. Decobert, P. L. Barny, S. Esselin, C. Friedrich and C. Noël, *Mol. Cryst. Liq. Cryst.*, 1986, **137**, 349-364.
27 N. Lacoudre, A. L. Borgne, N. Spassky, J. P. Vairon, P. L. Barny, J. C. Dubois, S. Esselin, C. Friedrich and C. Noël, *Mol. Cryst. Liq. Cryst.*, 1988, **155**: 113-127.
28 V. Percec, M. Lee. J. Heck, H. E. Blackwell, G. Ungar and A. Alvarez-Castillo *J. Mater. Chem.*, 1992, **2**, 931-938.
29 Y. F. Zhao, X. H. Fan, X. H. Wan, X. F. Chen, Yi, L. S. Wang, X. Dong and Q. F. Zhou, *Macromolecules*, 2006, **39**, 948-956.
30 Z. N. Yu, H. L. Tu, X. H. Wan, X. F. Chen and Q. F. Zhou, *J. Polym. Sci. Part A: Polym. Chem.*, 2003, **41**, 1454-1464.
31 Z. G. Zhu, J. G. Zhi, A. H. Liu, J. X. Cui, X. H. Wan and Q. F. Zhou, *J. Polym. Sci. Part A: Polym. Chem.*, 2007, **45**, 830–847.
32 Y. F. Zhu, H. J. Tian, H. W. Wu, D. Z. Hao, Y. Zhou, Z. H. Shen, D.C. Zou, P. C. Sun, X. H. Fan and Q. F. Zhou, *J. Polym. Sci. Part A: Polym. Chem.*, 2014, **52**, 295-304.
33 X. Y. Yin, C. Ye, X. Ma, E. Q. Chen, X. Y. Qi, X. F. Duan, X. H. Wan, S. Z. Cheng and Q. F. Zhou, *J. Am. Chem. Soc.*, 2003, **125**, 6854-6855.

34 D. Zhang, Y. X. Liu, X. H. Wan and Q. F. Zhou, *Macromolecules*, 1999, **32**, 5183-5185.
35 S. Chen, J. Qiu, H. L. Xie and H. L. Zhang, *J. Polym. Sci. Part A: Polym. Chem.*, 2013, **51**, 2804-2816.
36 L. Y. Zhang and Y. F. Zhang, *J. Polym. Sci. Part A: Polym. Chem.*, 2013, **51**, 2545-2554.
37 X. Q. Liu, J. Wang, S. Yang, Y. F. Men, P. C. Sun and E. Q. Chen, *Polymer*, 2016, **87**, 260-267.
38 Y. F. Zhu, X. L. Guan, Z. H. Shen, X. H. Fan and Q. F. Zhou, *Macromolecules*, 2012, **45**, 3346−3355.
39 Y. B. Luo, S. Chen and H. L. Zhang, *RSC Adv.*, 2015, **5**, 54920-54928.
40 S. George and A. Sudalai, *Tetrahedron-Asymmetry*, 2007, **18**, 975-981.
41 Y. Bikard, J. M. Weibel, C. Sirlin, L. Dupuisc, J. P. Loefflerc and P. Palea, *Tetrahedron Lett*., 2007, 48, 8895-8899.
42 S. Chen, X. Shu, H. L. Xie and H. L. Zhang, *Polymer*, 2013, **54**, 3556-3565.
43 G. L. Jiang, H. H. Cai, Z. H. Shen, X. H. Fan and Q. F. Zhou, *J. Polym. Sci. Part A: Polym. Chem.*, 2013, **51**, 557-564.
44 X. F. Chen, Z. H. Shen, X. H. Wan, X. H. Fan, E. Q. Chen, Y. G. Ma and Q. F. Zhou, *Chem. Soc. Rev.*, 2010, **39**, 3072-3101.
45 S. T. Sun, H. Tang, P. Y. Wu and X. H. Wan, *Phys. Chem. Chem. Phys.*, 2009, **11**, 9861–9870.

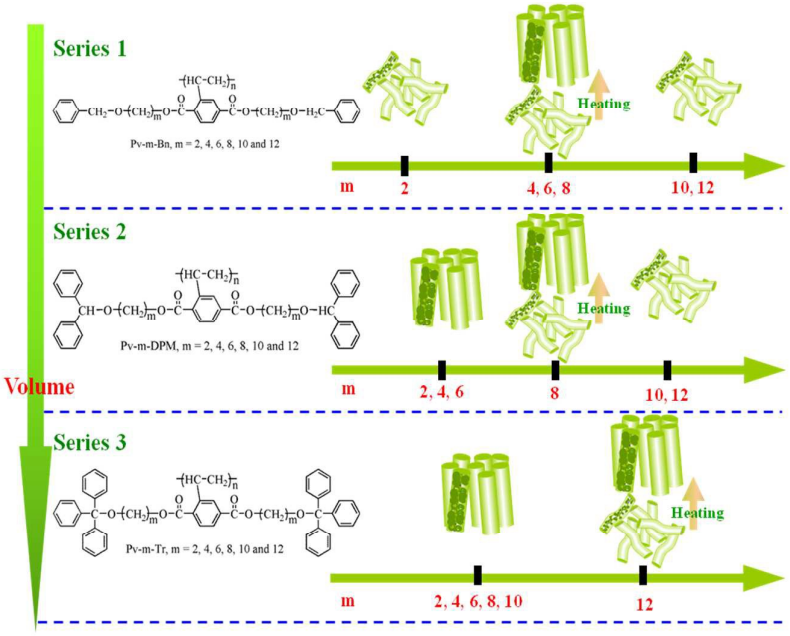

Graphical Abstract:

The alkyl spacer length and the terminal group volume influence on the phase behavior and structure of mesogen-jacketed liquid-crystalline polymers